Flavonols control pollen tube growth and integrity by regulating ROS homeostasis during high-temperature stress

Joëlle K. Muhlemann[a], Trenton L. B. Younts[a], and Gloria K. Muday[a,b,1]

[a]Department of Biology, Wake Forest University, Winston-Salem, NC 27109; and [b]Center for Molecular Signaling, Wake Forest University, Winston-Salem, NC 27109

Edited by June B. Nasrallah, Cornell University, Ithaca, NY, and approved October 15, 2018 (received for review July 6, 2018)

Plant reproduction requires long-distance growth of a pollen tube to fertilize the female gametophyte. Prior reports suggested that mutations altering synthesis of flavonoids, plant specialized metabolites that include flavonols and anthocyanins, impair pollen development in several species, but the mechanism by which flavonols enhanced fertility was not defined. Here, we used genetic approaches to demonstrate that flavonols enhanced pollen development by reducing the abundance of reactive oxygen species (ROS). We further showed that flavonols reduced high-temperature stress-induced ROS accumulation and inhibition of pollen tube growth. The *anthocyanin reduced* (*are*) tomato mutant had reduced flavonol accumulation in pollen grains and tubes. This mutant produced fewer pollen grains and had impaired pollen viability, germination, tube growth, and tube integrity, resulting in reduced seed set. Consistent with flavonols acting as ROS scavengers, *are* had elevated levels of ROS. The pollen viability, tube growth and integrity defects, and ROS accumulation in *are* were reversed by genetic complementation. Inhibition of ROS synthesis or scavenging of excess ROS with an exogenous antioxidant treatment also reversed the *are* phenotypes, indicating that flavonols function by reducing ROS levels. Heat stress resulted in increased ROS in pollen tubes and inhibited tube growth, with more pronounced effects in the *are* mutant that could be rescued by antioxidant treatment. These results are consistent with increased ROS inhibiting pollen tube growth and with flavonols preventing ROS from reaching damaging levels. These results reveal that flavonol metabolites regulate plant sexual reproduction at both normal and elevated temperatures by maintaining ROS homeostasis.

heat stress | reactive oxygen species | flavonols | pollen | ROS

During sexual reproduction in plants, male sperm cells located in the pollen grain are delivered to the female gametophyte. This process occurs through the formation of a pollen tube that emerges from the pollen grain and grows through the female organ, the pistil, to reach and fertilize the female gametophyte located inside the ovule (1). Reactive oxygen species (ROS) serve as one of multiple signaling molecules during pollen development and differentiation (2–9). ROS have been implicated in reproduction, predominantly in *Arabidopsis thaliana* and tobacco, with effects on male gametophyte development (2), pollen germination (3, 4), pollen tube growth (5–7), and tube burst during fertilization (8).

Maintenance of ROS homeostasis is a key feature of productive ROS signaling, as intermediate levels of ROS positively regulate signaling, while high levels have cytotoxic effects. ROS often reach high levels as a result of abiotic stress, so cells have active mechanisms to keep ROS at signaling concentrations to prevent toxicity (10). To maintain ROS homeostasis, plants use diverse enzymatic and nonenzymatic antioxidant machineries (11), including flavonols and anthocyanin metabolites, which are part of the larger flavonoid family (12). Flavonols are ubiquitous plant specialized metabolites with varying degrees of hydroxylation on their phenolic ring moiety (12), which allows them to accept electrons and thereby act as antioxidants (13, 14). Flavonols serve as precursors for the synthesis of anthocyanins, which are pigments conferring color to diverse fruits and flowers (12). The presence (or absence in mutants) of colored anthocyanins has enabled the identification of the biochemical sequence and regulatory genes controlling flavonol and anthocyanin biosynthesis (12, 15). These mutant genotypes have also been used to demonstrate the function of flavonols in diverse plant growth, developmental, and physiological processes (16), including root development and gravitropism (17–20), leaf and trichome development (21, 22), and stomatal aperture (23, 24). Consistent with the antioxidant activity of flavonols in vivo, mutants with decreased levels of flavonols contain elevated levels of ROS in root hairs and guard cells, where they enhance root hair development (25) and stimulate stomatal closure (23, 24). In several crop species, such as maize, petunia, tobacco, and tomato—although not in *Arabidopsis*—flavonols are also necessary for pollen viability, germination, and tube growth (26–31), and thereby promote successful plant reproduction.

Pollen development and tube growth are extremely sensitive to deviations from optimal temperatures. The inhibitory effects of high temperature on cotton, maize, and tomato pollen are well described (32–37). Indeed, acute heat stress during the pollen tube growth phase has the potential to completely block seed and fruit production, which can result in substantial reductions in

Significance

Plant sexual reproduction is required for seed and fruit production and is highly sensitive to elevated temperatures, suggesting that climate change may have profound agricultural impacts through inhibition of this process. During reproduction, pollen tubes must navigate long distances through floral tissues to fertilize ovules. We demonstrate that high-temperature stress increases levels of reactive oxygen species in pollen tubes, which inhibits pollen tube growth. We report that specialized metabolites of the flavonol class prevent reactive oxygen species from reaching inhibitory levels at normal and increased temperatures, thereby promoting pollen viability and pollen tube growth. These results indicate that flavonols enhance reproduction, particularly during heat stress, and could confer protection to plants against the negative effects of climate change.

Author contributions: J.K.M. and G.K.M. designed research; J.K.M. and T.L.B.Y. performed research; J.K.M. and T.L.B.Y. analyzed data; and J.K.M. and G.K.M. wrote the paper.

The authors declare no conflict of interest.

This article is a PNAS Direct Submission.

[1]To whom correspondence should be addressed. Email: muday@wfu.edu.

This article contains supporting information online at www.pnas.org/lookup/suppl/doi:10.1073/pnas.1811492115/-/DCSupplemental.

Published online November 9, 2018.

crop yield (33, 34). Heat stress increases ROS production, which results in distinct transcriptional responses (38), including increased abundance of transcripts and proteins involved in ROS scavenging (39–41). Elevated temperature has been shown to increase flavonol biosynthesis in vegetative tissues (39), as well as in developing pollen (42). However, the involvement of flavonols as antioxidants against high-temperature–induced ROS has not been reported.

This work tests the possibility that flavonols control pollen germination and tube growth by regulating ROS homeostasis. The *anthocyanin reduced* (*are*) mutant, which lacks a functional flavonol 3-hydroxylase (F3H) enzyme (25, 43), produced fewer viable pollen grains, displayed a reduced pollen germination rate, and slower pollen tube growth. These phenotypes were complemented in transgenics expressing the *F3H* gene. Flavonols accumulated in wild-type pollen grains and tubes and were at lower levels in the *are* mutant. The abundance of total ROS and H_2O_2 in pollen grains and tubes were elevated in the *are* mutant, suggesting that flavonols act as ROS scavengers in reproductive tissues. Treatments that block ROS synthesis or that scavenge ROS rescued the pollen tube growth and integrity defects in the *are* mutant, consistent with flavonols controlling pollen tube growth through their ROS scavenging properties. Finally, extended heat stress during flower development reduced pollen viability, with more pronounced effects in the *are* mutant. Acute heat stress in pollen tubes elevated ROS levels and inhibited growth of pollen tubes and pollen tube integrity. These effects on pollen tubes were more pronounced in the *are* mutant and reversed by antioxidant treatment. This work reveals a role for flavonols as ROS scavengers in pollen under normal and abiotic stress conditions.

Results

Flavonols Regulate Seed Set in Tomato. To assess the role of flavonols in sexual reproduction in tomato, we first analyzed fruit weight and seed set in wild-type (VF36) and the *are* mutant. A point mutation in the *F3H* gene results in an early stop codon in the *are* mutant (44). This leads to reduced accumulation of flavonols and anthocyanins and increased accumulation of naringenin, the F3H substrate, in vegetative tissues (25). In greenhouse-grown plants, we found that seed set was significantly reduced by 2.9-fold in the *are* mutant (Fig. 1*B*). Fruit size is often slightly smaller in the *are* mutant (Fig. 1*A*), but because of size variability, the average weight in the *are* mutant was not statistically significantly different from the parental line VF36 (Fig. 1*C*). This result suggests that the differences in seed set between *are* and VF36 are not the result of altered fruit size.

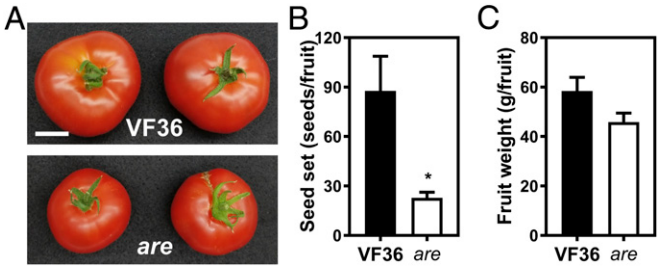

Fig. 1. Flavonols regulate seed set in tomato. (*A*) Ripe tomato fruits of the wild-type VF36 and the *are* mutant. (Scale bar, 3 cm.) (*B*) Quantification of seed set in VF36 and the *are* mutant. (*C*) Quantification of fruit weight in VF36 and the *are* mutant. (*B* and *C*) Data are the mean ± SEM of 10 fruits. The asterisk indicates a significant difference between VF36 and the *are* mutant, according to a Student's *t* test with $P < 0.05$.

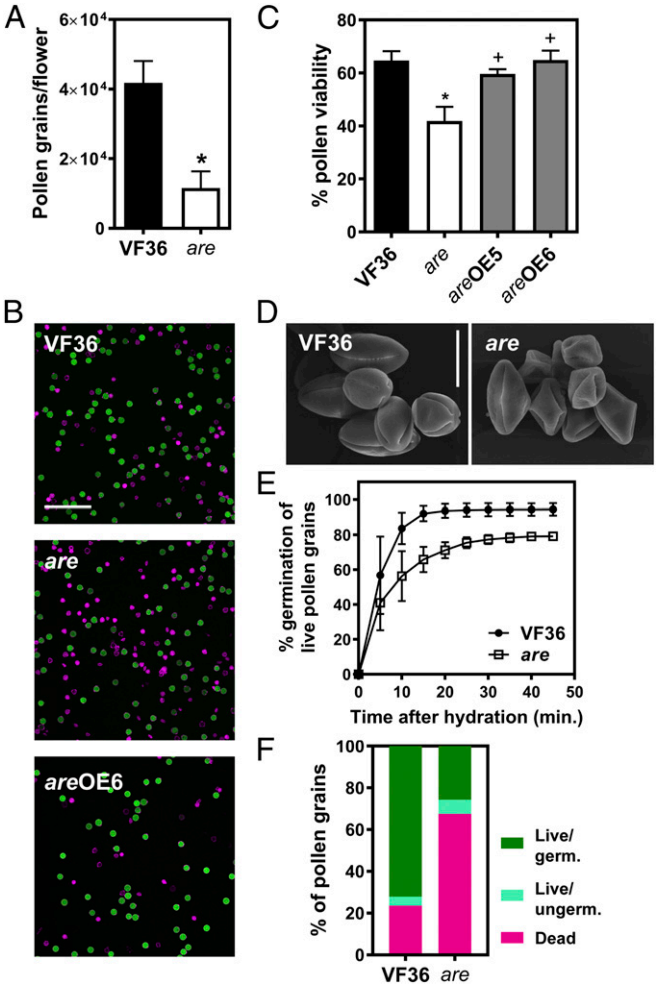

Fig. 2. Flavonols control pollen viability and germination in tomato. (*A*) Quantification of pollen grains in VF36 and the *are* mutant. Pollen grains per flower were quantified by flow cytometry. Data are mean ± SEM of three independent experiments with two to three flowers per experiment. (*B*) Confocal micrographs of VF36, *are*, and *are-35S:F3H* complementation line #6 pollen grains stained with FDA (live pollen grains, shown in green) and PI (dead pollen grains, shown in magenta). (Scale bar, 200 μm.) (*C*) Quantification of pollen viability in VF36, *are*, and *are-35S:F3H* complementation lines. Data are shown as the mean ± SEM of two independent experiments. Asterisks indicate significant differences between VF36 and other genotypes and plus signs differences between *are* and complementation lines, according to an ANOVA followed by a Šídák post hoc test with $P < 0.05$. (*D*) Scanning electron micrographs of VF36 and *are* pollen grains collected at anthesis. (Scale bar, 20 μm.) (*E*) Quantification of germination rates in VF36 and the *are* mutant. Data are shown as the mean ± SEM of three independent experiments. (*F*) Summary of pollen viability and germination rates in VF36 and the *are* mutant.

Pollen Viability and Germination Are Impaired in the Flavonol-Deficient *are* Tomato Mutant. To better understand the contribution of flavonols to fertility in tomato, we quantified pollen yield, viability, and germination in VF36 and the *are* mutant. Pollen grains were harvested at anthesis and quantified by flow cytometry in plants grown in standard conditions. The quantity of pollen released from VF36 anthers was 3.6-fold greater than from *are* mutant anthers (Fig. 2*A*). Consistent with this lower pollen yield in *are*, to recover equivalent amounts of pollen we had to use three to four times as many flowers from *are* as from VF36 plants to isolate equivalent amounts of pollen for experimentation.

Pollen viability was assessed by staining pollen grains with fluorescein diacetate (FDA) (Fig. 2*B*, green) and propidium iodide (PI) (Fig. 2*B*, magenta). In viable pollen grains, FDA is converted to fluorescein by cytoplasmic esterase activity and PI labels pectin in cell walls. Dead pollen grains are characterized by an absence of esterase activity and thus lack fluorescein-derived fluorescence and become permeable to PI, therefore displaying PI fluorescence inside the grain. This staining approach revealed that pollen viability is reduced by 35.2% in the *are* mutant compared with VF36 (Fig. 2 *B* and *C*). To verify that this phenotype is directly tied to the *are* mutation, the viability of the *are* mutant complemented with the wild-type *F3H* gene under control of the *CaMV 35S* promoter (25) was examined. In two independently transformed lines, pollen viability was restored to wild-type levels (Fig. 2*C*), consistent with this phenotype being linked to the *are* mutation. In addition to having reduced viability, *are* mutant pollen grains collected at anthesis displayed a collapsed phenotype, while VF36 had normally shaped grains (Fig. 2*D*).

A time course of pollen germination was conducted for VF36 and *are* and germination is reported relative to the total number of live pollen grains (Fig. 2*E*). This time course revealed that the *are* mutant had a lower percentage of pollen germination than VF36 at all time points and that within 30 min, both genotypes reached their maximum germination (Fig. 2 *E* and *F*). To illustrate and summarize the effects of reduced flavonols in pollen, the relative abundance of live and germinated pollen grains, live and ungerminated pollen grains, and dead pollen grains for VF36 and the *are* mutant are shown in Fig. 2*F*. This highlights the combined effects of pollen failure at multiple stages, showing that only 26% of the pollen grains in the *are* mutant germinated, while 72% of VF36 pollen grains germinated. Taken together, these results point to a role for flavonols in male gametophyte development in tomato.

Flavonols Enhance Pollen Tube Growth and Integrity. The effect of the *are* mutation on elongation of pollen tubes was examined in tubes grown in vitro at 28 °C for 4 h. Pollen tubes of the *are* mutant were 40% shorter than VF36 (Fig. 3 *A* and *B*). Genetic complementation of the *are* mutant with the *35S:F3H* transgene rescued pollen tube growth to levels observed in VF36, suggesting that the *F3H* mutation underlies the defective pollen tube growth phenotype in the *are* mutant. We also observed morphological changes in *are* pollen tubes, including swelling at the tip (Fig. 3*C*) and impaired integrity of the tube, resulting in rupture of tubes, as shown in examples in Fig. 3*E*. Percentage of intact tubes was quantified in VF36, the *are* mutant, and the complemented lines (Fig. 3*D*). The prevalence of ruptured pollen tubes (i.e., those that are not intact) was significantly increased by 2.4-fold in the *are* mutant over VF36 and this phenotype was rescued by genetic complementation of the *are* mutant (Fig. 3*D*). The multiple pollen defects observed in the *are* mutant likely underlie the reduced seed set phenotype of the *are* mutant and are reversed by complementation, suggesting that reduced flavonol synthesis underlies these defects.

Flavonols Accumulate in Pollen Grains and Tubes at Reduced Levels in the *are* Mutant. We examined the localization of flavonols in pollen grains and tubes using the flavonol-specific dye diphenylboric acid-2-aminoethyl ester (DPBA) (20). The fluorescence pattern was examined by laser-scanning confocal microscopy (LSCM). Pollen grains and tubes stained with DPBA show bright fluorescence consistent with flavonols localizing to these cell structures. We did not observe a fluorescence signal under the same imaging conditions in the absence of DPBA. Interestingly, DPBA fluorescence was lower at germination pores, indicated by an arrow in Fig. 4*A*, which have previously been suggested to be sites of elevated ROS (3, 4), suggesting that there are cellular mechanisms that lead to localized accumulation of these antioxidants to modulate ROS at these positions.

Detection of DPBA fluorescence in pollen grains was consistent with the accumulation of flavonols in pollen, as judged by liquid chromatography-mass spectrometry (LC-MS) (*SI Appendix*, Fig. S1). In contrast, anthocyanins, which are downstream metabolites in the flavonoid biosynthesis pathway, did not accumulate in pollen, as evidenced by spectrophotometric analysis (*SI Appendix*, Fig. S1). However, hypocotyl tissue accumulated anthocyanins (*SI Appendix*, Fig. S1).

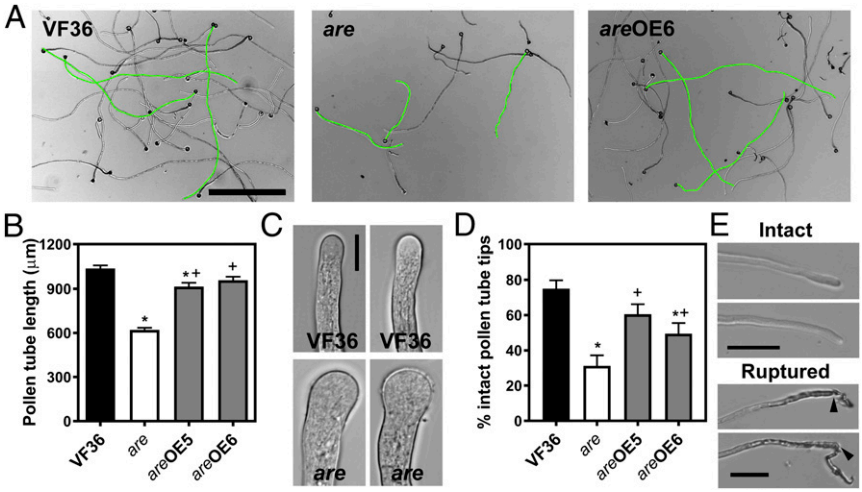

Fig. 3. Flavonols regulate pollen tube growth and integrity in tomato. (*A*) Bright-field images of VF36, *are*, and *are-35S:F3H* complementation line #6 pollen tubes grown in vitro for 4 h. (Scale bar, 500 μm.) Several pollen tubes of each phenotype are highlighted in green. (*B*) Quantification of in vitro pollen tube length after 4 h of growth in VF36, *are*, and *are-35S:F3H* complementation lines. Data are shown as the mean ± SEM. $n = 127–140$ tubes measured across three independent experiments. (*C*) Bright-field images of pollen tube tips. (Scale bar, 10 μm.) (*D*) Quantification of pollen tubes with burst tips in VF36, *are*, and *are-35S:F3H* complementation lines after 4 h of pollen tube growth. Data are mean ± SEM. (*B* and *D*) Asterisks indicate significant differences between VF36 and other genotypes and plus signs indicate differences between *are* and complementation lines, according to an ANOVA followed by a Šídák post hoc test with $P < 0.05$. (*E*) Bright-field images illustrate pollen tubes with intact and ruptured tips. Black arrows indicate points of rupture at the pollen tube tip. (Scale bars, 50 μm.)

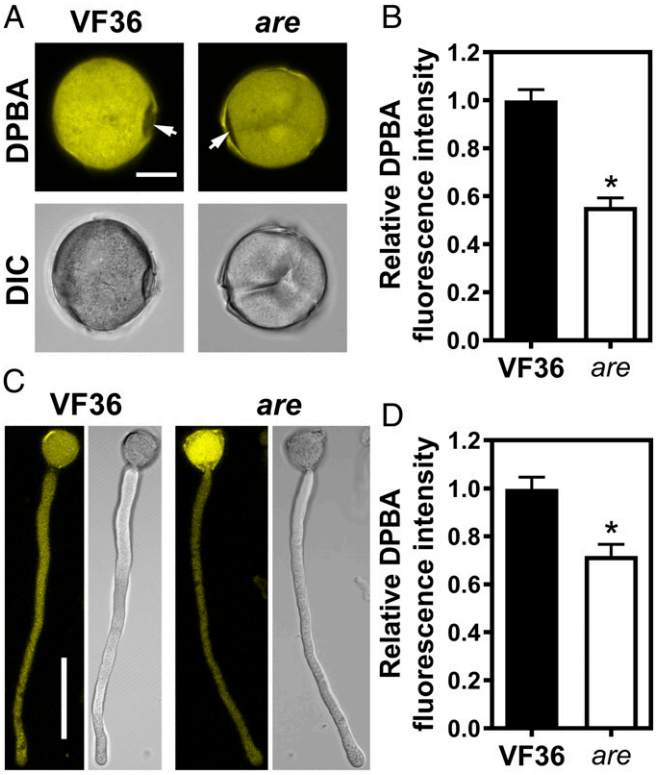

Fig. 4. Flavonols accumulate in tomato pollen grains and tubes and are decreased in pollen of the *are* mutant. (*A*) Confocal micrographs and differential interference contrast (DIC) images showing DPBA fluorescence in pollen grains of the wild-type VF36 and *are* tomato mutant. The arrows points to the pollen aperture. (Scale bar, 10 μm.) (*B*) Quantification of DPBA fluorescence intensity in grains of VF36 and the *are* mutant. Data are shown as the mean ± SEM. n = 48–106 grains measured across three independent experiments. The asterisk indicates a significant difference between VF36 and the *are* mutant, according to a Student's t test with $P < 0.05$. (*C*) Confocal micrographs and DIC images showing DPBA fluorescence in pollen tubes of VF36 and the *are* mutant. (Scale bar, 50 μm.) Confocal micrographs show the maximum intensity projection of DPBA fluorescence. (*D*) Quantification of DPBA fluorescence in pollen tubes of VF36 and the *are* mutant using maximum intensity projections of *z*-stacks. Data are the mean ± SEM. n = 30 tubes measured across three independent experiments. The asterisk indicates a significant difference between VF36 and the *are* mutant, according to a Student's t test with $P < 0.05$.

We evaluated whether the *are* mutant has reduced flavonols in pollen grains and tubes. Previous analysis of flavonol metabolite pools by LC-MS in roots, hypocotyls, and leaves of the *are* mutant showed that the mutation in *F3H* reduces flavonol biosynthesis and increases the pool size of the F3H substrate naringenin (24, 25). Similar LC-MS analyses are not feasible in *are* pollen, as the proportions of viable pollen in VF36 and the *are* mutant are different and we would thus not compare similar populations of pollen. However, quantification of DPBA fluorescence intensity in pollen grains and tubes of the *are* mutant revealed that flavonol levels were significantly reduced by 1.8- and 1.4-fold, respectively, compared with wild-type grains and tubes (Fig. 4). As pollen grains did not accumulate anthocyanins (*SI Appendix*, Fig. S1), the metabolic changes and phenotypic defects in the *are* mutant are linked to altered flavonol levels.

ROS Levels Are Regulated by Flavonols in Tomato Pollen Grains and Tubes. We examined the distribution of ROS in pollen grains and tubes using two ROS sensors. The general ROS sensor 5-(and 6)-chroromethyl-2′,7′-dichlorodihydrofluorescein diacetate (CM-H_2DCFDA), which is converted to the highly fluorescent 2′,7′-dichlorofluorescein (DCF) upon oxidation by ROS, was used to visualize and quantify total ROS. Using LSCM, we collected single optical slices to visualize ROS in pollen grains and quantified DCF signal in the entire grain from these images. For pollen tubes, *z*-stacks were collected and DCF signal was quantified in the complete pollen tube using maximum intensity projections of the *z*-stacks. We detected bright DCF signal intensity in grains, with elevated levels at the germination pores (Fig. 5*A*). The DCF signal was also evident in the pollen tube where it was brightest at the tip (Fig. 5 *E* and *F*). To determine whether flavonols modulate ROS levels in tomato pollen grains and tubes, we compared DCF fluorescence in the *are* mutant to VF36. DCF fluorescence intensity was 2.6- and 4.0-fold higher in *are* mutant pollen grains and tubes, respectively, than in wild-type (Fig. 5 *B* and *E*). DCF fluorescence intensity was reduced to wild-type levels in the *are* mutant genetically complemented with the *35S:F3H* construct (Fig. 5*E*).

Prior reports have indicated that there is tip-localized ROS production driven by tip-localized NADPH oxidases that are necessary for pollen tube growth (5–7). Quantification of ROS gradients along the pollen tube—from tip to shank—allowed us to ask whether flavonols play a role in establishing these gradients. In wild-type, DCF fluorescence intensity at the tip was 1.2-fold higher 0–30 μm from the tip than 100–130 μm behind the tip (Student's t test: $t = 6.99$, $P < 0.001$). Reduced flavonol levels in the *are* mutant led to a steeper gradient in CM-H_2DCFDA staining along the pollen tube compared with VF36 (Fig. 5*F*), with a 1.4-fold difference from tip to base. The largest genotypic differences in fluorescence intensity was observed at the tip of the pollen tube, with a 3.6-fold difference in DCF fluorescence intensity between VF36 and the *are* mutant 0–25 μm from the tip. This difference was smaller 125–150 μm behind the tip, where it is reduced to a 2.9-fold difference (Fig. 5*F*).

To eliminate the possibility that there were differences in dye uptake between VF36 and *are* genotypes, we performed staining with the dye FDA. FDA is structurally similar to CM-H_2DCFDA, but has not been reported to be ROS sensitive. FDA fluorescence intensity in VF36 and *are* pollen tubes was not significantly different ($P = 0.35$), consistent with similar dye uptake in both genotypes (*SI Appendix*, Fig. S2). Additionally, we asked if there was a tip-focused FDA gradient in VF36 by comparing the best-fit values from one phase decay modeling of the gradient and find that the FDA gradient is significantly shallower than the DCF gradient (Dataset S1). Additionally, the reduced DPBA fluorescence in *are* further supports the hypothesis that dye uptake is not enhanced in this mutant. These results suggest that the increase in DCF signal in *are* is due to elevated ROS, not a dye uptake difference.

To visualize localization of hydrogen peroxide, we used the H_2O_2-specific probe Peroxy Orange 1 (PO1) (Fig. 5 *C*, *D*, and *G*). PO1 fluorescence is pronounced at the cell membrane and cell wall of pollen grains (Fig. 5*C*). Compared with DCF, which localizes to the pore, PO1 fluorescence is visible around the pore and absent at the pore itself (Fig. 5*C*). This localization is consistent with a prior report suggesting that hydrogen peroxide accumulates around these structures (4). PO1 was used to image pollen tubes as well (Fig. 5*G*). Because the signal is much weaker in the tubes, images were captured with the pollen grains showing saturating levels of PO1. In contrast to DCF, this dye shows more uniform distribution of hydrogen peroxide along the growing pollen tube (Fig. 5*H*). PO1 fluorescence in *are* pollen grains and tubes was 1.2- and 1.3-fold increased, respectively, compared with the levels in VF36 pollen grains and tubes (Fig. 5 *D* and *G*). PO1 also showed a gradient from tip to shank in VF36 and *are*, with a 1.2- and 1.3-fold difference from tip to shank, respectively (Student's t test: $t = 9.46$, $P < 0.001$). However, when PO1 fluorescence was compared at either end of the

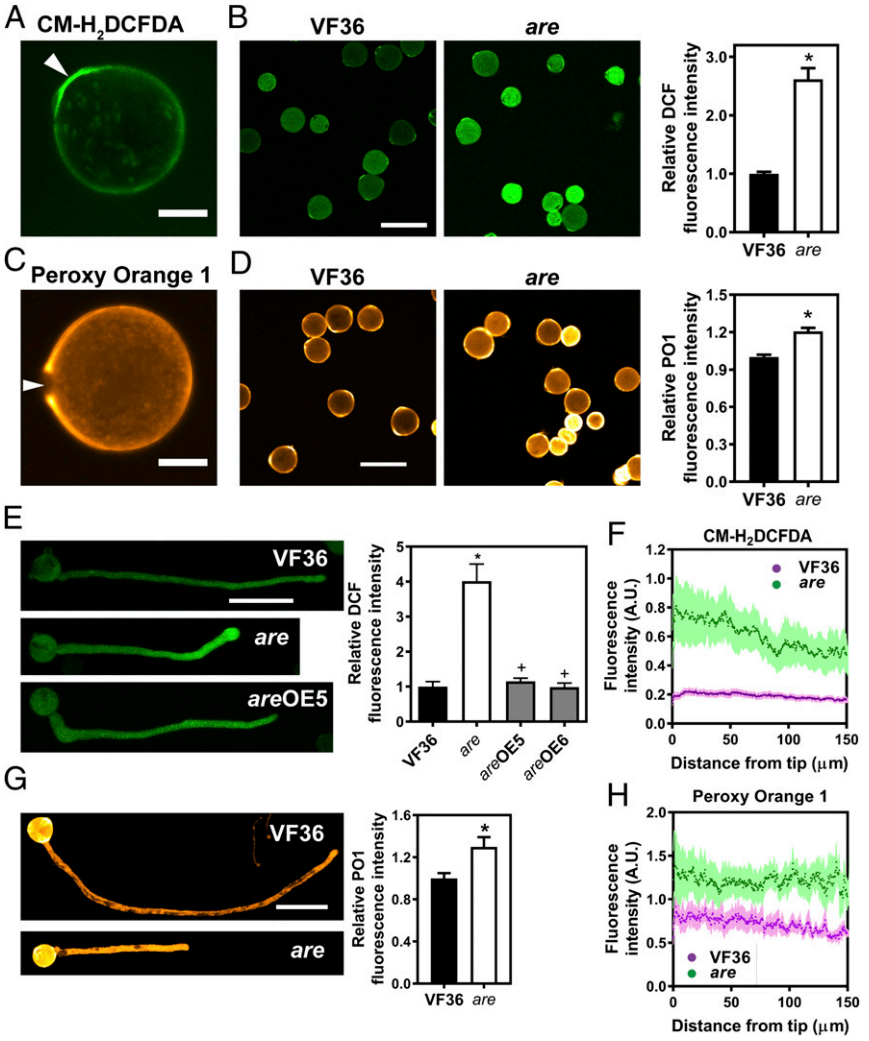

Fig. 5. ROS levels are increased in the *are* mutant. (*A*) Confocal micrograph of a VF36 (wild-type) pollen grain stained with the generic ROS sensor CM-H_2DCFDA. (Scale bar, 10 μm.) (*A* and *C*) Arrows point to the pollen aperture. (*B*) Confocal micrographs of VF36 and *are* mutant pollen grains stained with CM-H_2DCFDA. (Scale bar, 50 μm.) The graph represents quantification of DCF fluorescence in pollen grains of VF36 and the *are* mutant. (*B*, *D*, and *G*) Data are the mean ± SEM. Asterisks indicate significant differences between VF36 and the *are* mutant, according to a Student's *t* test with $P < 0.05$. (*C*) Confocal micrograph of a VF36 pollen grain stained with the hydrogen peroxide-specific probe PO1. (Scale bar, 10 μm.) (*D*) Confocal micrographs of VF36 and *are* mutant pollen grains stained with PO1. (Scale bar, 10 μm.) The graph represents quantification of PO1 fluorescence in pollen grains of VF36 and the *are* mutant. (*E*) Confocal micrographs of VF36, *are* and *are-35S:F3H* complementation line #5 pollen tubes stained with CM-H_2DCFDA. (Scale bar, 50 μm.) Quantification of DCF fluorescence in pollen tubes of VF36, *are*, and *are-35S:F3H* complementation lines. Data are shown as the mean ± SEM. $n = 20$–26 tubes measured across two independent experiments. Asterisks indicate significant differences between VF36 and other genotypes and plus signs differences between *are* and complementation lines, according to an ANOVA followed by a Šídák post hoc test with $P < 0.05$. (*F* and *H*) Quantification of CM-H_2DCFDA and PO1 fluorescence along pollen tubes of VF36 and *are*, respectively. Dotted lines represent the average fluorescence for 10 pollen tubes, while lightly shaded areas represent the SEM. (*G*) Confocal micrographs of pollen tubes stained with PO1. (Scale bar, 100 μm.) The graph represents quantification of PO1 fluorescence in maximum intensity projections of *z*-stacks in pollen tubes of VF36 and the *are* mutant.

gradient, there was less difference between VF36 and the *are* mutant (1.6- and 1.9-fold difference at the tip and 125–150 μm behind the tip, respectively) (Fig. 5*H*) than observed with DCF staining.

Pollen Tube Growth and Integrity Defects in the *are* Mutant Are Rescued by Scavenging of Excess ROS and Inhibition of ROS Production, Respectively. To test if the increased levels of ROS underlie tube growth and integrity defects in *are* mutant pollen, we scavenged excess ROS using the antioxidant ascorbic acid or reduced ROS synthesis by inhibition of NADPH oxidase with diphenylene iodinium (DPI) and examined the effect of these treatments. The statistical significance of these treatments was determined by ANOVA followed by a Fisher's least-significant difference (LSD) post hoc test and the output of those statistical tests is reported in Dataset S2. Supplementing the pollen germination medium with ascorbic acid significantly increased the length of *are* pollen tubes ($P = 0.03$), consistent with an inhibition of pollen tube length by excess ROS (Fig. 6*A*). However, this treatment significantly decreased length of VF36 pollen tubes, consistent with reductions of ROS to suboptimal levels in this genotype (Fig. 6*A*). Treatment with the NADPH oxidase inhibitor DPI did not significantly change pollen tube length in VF36 and the *are* mutant ($P = 0.19$ and 0.79, respectively) (Fig. 6*A*).

To examine effects of flavonols and ROS on pollen tube integrity, we quantified the percentage of intact pollen tubes after 4 h of pollen tube growth in pollen germination medium with

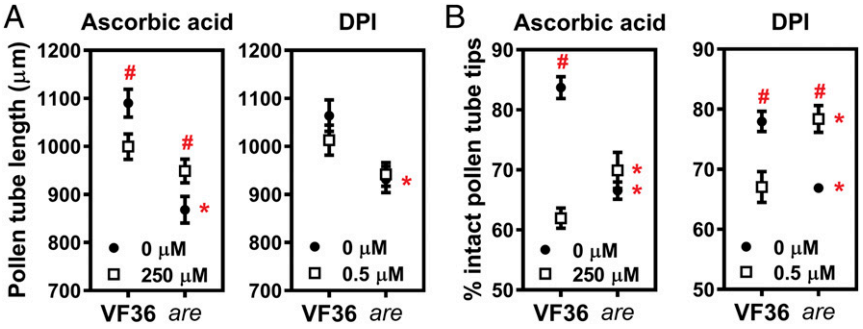

Fig. 6. Antioxidant treatment and inhibition of ROS synthesis rescue defects in pollen tube growth and integrity caused by reduced flavonol levels. (*A*) Quantification of in vitro tube growth in VF36 and the *are* mutant grown for 4 h at 28 °C. Supplementation of the pollen germination medium with the nonenzymatic antioxidant ascorbic acid or the NADPH oxidase inhibitor DPI occurred after 90 min of growth. Data represent mean ± SEM. $n = 80$ tubes measured across two independent experiments. (*B*) Quantification of pollen tube integrity in VF36 and the *are* mutant. Data originate from the same pollen samples as in Fig. 5*A*, but have different solvent controls, as outlined in the methods. Data represent mean ± SEM. The error bar is shorter than the height of the symbol for tube integrity in the *are* mutant treated with 0 μM DPI. Integrity was assessed in more than 150 pollen tubes for each condition and genotype across two independent experiments. In *A* and *B*, asterisks indicate significant differences between VF36 and *are* within the same concentration of ascorbic acid or DPI, and pound signs highlight differences between concentrations within the same genotype, according to two-way ANOVA followed by a Fisher's LSD test with $P < 0.05$.

and without ascorbic acid or DPI. Treatment with DPI resulted in a significant increase in pollen tube integrity in the *are* mutant compared with untreated *are* ($P = 0.005$), with the effects of DPI converting the number of intact pollen tubes to levels not significantly different from untreated VF36 ($P = 0.92$) (Fig. 6*B* and Dataset S3). These results suggest that tip-localized ROS synthesized by NADPH oxidases cause the rupture of *are* pollen tubes. Ascorbic acid and DPI treatments compromised pollen tube integrity in VF36 (Fig. 6*B* and Dataset S3), again consistent with reduction in ROS to suboptimal levels.

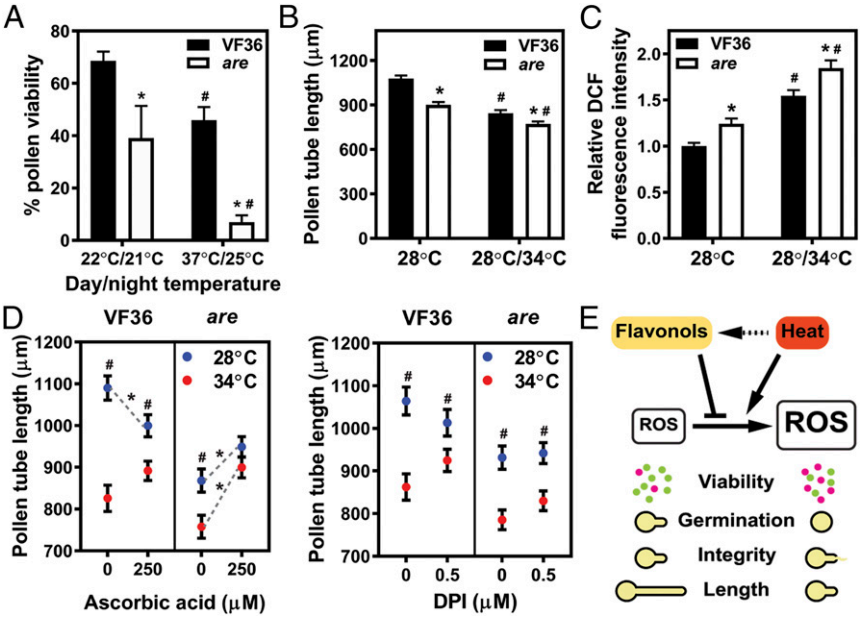

Fig. 7. Flavonols regulate pollen viability, tube length, and ROS levels during heat stress. (*A*) Quantification of pollen viability in VF36 and the *are* mutant grown in two different greenhouse temperature regimes. (*A*–*C*) Data are shown as the mean ± SEM. Asterisks indicate significant differences between VF36 and *are* and pound signs indicate differences between temperature treatments, according to two-way ANOVA followed by a Fisher's LSD test with $P < 0.05$. (*B*) Quantification of in vitro tube growth in VF36 and the *are* mutant at two different temperature regimes. Pollen tubes were grown in germination medium for 90 min at 28 °C and then for 150 min at 34 °C or kept at 28 °C for another 150 min. $n = 166$–168 tubes measured across three independent experiments. (*C*) Quantification of DCF fluorescence in pollen tubes of VF36 and *are* grown in vitro at the two different temperature regimes described above. $n = 97$–123 tubes measured across four independent experiments. (*D*) Quantification of pollen tube length in VF36 and the *are* mutant. Pollen tubes of VF36 and the *are* mutant were grown for 90 min at 28 °C and then transferred for 150 min to 34 °C (red symbols) or kept for another 150 min at 28 °C (blue symbols). Supplementation of the pollen germination medium with the nonenzymatic antioxidant ascorbic acid or the NADPH oxidase inhibitor DPI occurred after 90 min of growth at 28 °C. Data represent mean ± SEM. $n = 80$ tubes measured across two independent experiments. Gray, dotted lines with asterisks indicate significant differences between control and treatment within the same genotype and temperature regime. Pound signs indicate significant differences in pollen tube length between 28 °C and 34 °C within the same genotype and treatment. (*E*) Model for the role of heat stress and flavonols in pollen viability, germination, and tube growth. Flavonols scavenge ROS produced in pollen at normal and increased temperatures, thereby regulating pollen viability, germination, and tube growth. Solid arrows depict relationships described in our study, whereas dashed arrows highlight relationships reported for vegetative tissues in the literature. Green dots represent viable pollen grains, while magenta dots are dead grains.

Flavonols Regulate Heat-Stress–Induced Reduction in Pollen Viability and Tube Growth and Increase in ROS. We examined the effects of prolonged heat stress on pollen viability. Pollen viability was assessed in VF36 and *are* mutant plants grown in a greenhouse in spring and summer, which exposed the plants to different temperature conditions. Average temperatures measured 7–15 d before anthesis in spring greenhouse conditions were 22 °C and 21 °C, for day and night, respectively, and in summer greenhouse conditions day and night temperatures were 37 °C and 25 °C, respectively. Elevated growing temperatures significantly decreased pollen viability in the wild-type VF36 by 33%, while elevated temperatures reduced pollen viability in the *are* mutant by 82% (Fig. 7*A*).

To analyze the role of ROS in the response to high temperature during pollen tube growth, we exposed pollen tubes of the wild-type VF36 to acute temperature stress. Pollen tubes of wild-type VF36 were exposed to 34 °C for 2.5 h after growing for 1.5 h at 28 °C. This treatment resulted in a 1.4-fold reduced tube length in VF36 compared with samples grown continuously at 28 °C for 4 h (Fig. 7*B*). Furthermore, high-temperature stress increased DCF fluorescence by 1.4-fold, as quantified by staining of pollen tubes with CM-H_2DCFDA (Fig. 7*C*). The *are* mutant had a 1.2-fold reduced pollen tube elongation at higher temperature compared with the 28 °C control, and this was associated with 1.5-fold higher levels of DCF fluorescence (Fig. 7 *B* and *C*), consistent with greater temperature sensitivity in this flavonol mutant.

To ask if the enhanced sensitivity of *are* to high-temperature–impaired pollen tube growth and integrity was due to elevated ROS, the antioxidant ascorbic acid was added to pollen tube growth media. Ascorbic acid ameliorated pollen tube growth defects caused by acute heat stress in the *are* mutant, leading to tube length that was not significantly different from the *are* 28 °C control ($P = 0.41$) or from the VF36 34 °C treatment ($P = 0.84$), but that were significantly increased over the *are* 34 °C control sample ($P = 0.0002$). Ascorbic acid significantly reduced pollen tube growth in VF36 at 28 °C, but not at 34 °C (Fig. 7*D* and Dataset S2), but these tubes were much longer than *are* tubes under this acute heat stress. In addition to inhibiting pollen tube growth, heat stress compromised pollen tube integrity in VF36 and the *are* mutant (*SI Appendix*, Fig. S3 and Dataset S3). However, this effect was not rescued by treatments with the same or higher doses of ascorbic acid (*SI Appendix*, Fig. S3 and Dataset S3).

The effect of treatments with the NADPH oxidase inhibitor DPI on tube length and integrity were examined in high-temperature–treated VF36 and *are* (Fig. 7*D* and *SI Appendix*, Fig. S3). DPI did not significantly change tube length or pollen tube integrity in VF36 and the *are* mutant grown at 34 °C (Fig. 7*D* and Datasets S2 and S3). The absence of a DPI effect on pollen tube growth and tube integrity during acute heat stress suggests that ROS produced through mechanisms other than NADPH oxidases are responsible for pollen tube growth inhibition and rupture during heat stress. This result differs from the DPI response at 28 °C where DPI decreased pollen tube integrity in VF36 pollen tubes grown at 28 °C (Fig. 6*B* and Dataset S3). This indicates that DPI has a net positive effect on pollen tube integrity during acute heat stress and that NADPH oxidase-derived ROS play a role in pollen tube integrity during this stress.

Discussion

Flavonols are plant specialized metabolites that occur ubiquitously across plant species (12). Characterization of flavonol biosynthetic mutants has highlighted the involvement of flavonols in diverse plant growth, developmental, and physiological processes (16). Flavonols have been shown to reduce levels of ROS and to affect signaling and development in guard cells, root, and leaf development (17–24). Interestingly, several studies have linked reduced flavonol levels to impaired fertility in petunia, maize, tobacco, and tomato. In these species, reduced flavonols resulted in decreased pollen viability, germination, and tube growth (26–30, 45). However, neither the localized accumulation of flavonols in pollen grains and tubes nor the mechanism linking reduced flavonol levels to impaired pollen function were reported in these studies. Here, we tested the hypothesis that flavonols help maintain ROS homeostasis, thereby controlling pollen viability, germination, and tube growth.

The accumulation and function of flavonols were examined in wild-type and the *are* tomato mutant, which has a defect in the *F3H* gene that leads to reduced flavonol and downstream anthocyanin accumulation (25). Because tomato pollen does not produce anthocyanins, this mutation only affects accumulation of flavonol pools in this tissue. We find that flavonols accumulate in pollen grains and tubes and that flavonol levels are decreased in *are* mutant pollen. The reduction in flavonol levels in the *are* mutant is associated with decreases in pollen quantity and viability, impaired pollen germination and tube growth, and compromised pollen tube integrity. These results suggest that in tomato, flavonols play important roles at diverse stages of pollen development. The pollen developmental and differentiation defects we observed in the *are* mutant translate into profound effects on reproductive success in the mutant, yielding fruits with substantially reduced seed set. This fruit phenotype was also observed in chalcone synthase (*CHS*) RNAi tomato plants, where reduction in *CHS* expression resulted in production of parthenocarpic fruit (28).

A central question of our study is whether flavonols control pollen viability and tube growth and integrity by regulating ROS levels. Flavonols possess potent in vitro antioxidant activity due to the presence of hydroxyl groups on their ring moieties (13, 14). ROS are important players in male gametophyte development (2), as well as in pollen germination and tube growth (5–7). However, excess ROS levels impair pollen tube germination (4, 7). These findings led to our hypothesis that maintenance of ROS homeostasis is a central determinant of normal pollen germination and tube growth. Consistent with this hypothesis, pollen grains and tubes of *are* have higher signal from a general ROS sensor CM-H_2DCFDA and the hydrogen peroxide-specific dye PO1. In tubes, ROS accumulated in a tip-focused gradient, which was accentuated in *are*. This gradient has been reported previously and suggested to result from production of ROS by tip-localized NADPH oxidases (5). The more substantial increases in DCF than PO1 in *are* suggest that ROS other than hydrogen peroxide might be the ROS scavenged by flavonols.

To determine whether elevated ROS levels measured in the *are* mutant cause the reduced pollen tube growth and integrity, we applied treatments that lower ROS levels. The nonenzymatic antioxidant ascorbic acid enhanced pollen tube growth in the *are* mutant (Fig. 5*A*), consistent with compensation for the absence of flavonol antioxidants. In contrast, the NADPH oxidase inhibitor DPI did not lead to statistically significant changes in *are* tube growth. These results suggest that overaccumulation of ROS produced through mechanisms other than NADPH oxidase inhibits tube growth in the *are* mutant. In contrast, DPI treatment in the *are* mutant restored pollen tube integrity to the levels observed in VF36, while ascorbic acid had a minimal effect on pollen tube integrity in the *are* mutant (Fig. 5*B*). This is consistent with localized overaccumulation of ROS at the pollen tube tip, likely the NADPH oxidase product, superoxide, driving increased tip rupture and with reduction in flavonols mediating this response. Our results on pollen tube growth and integrity suggest that different ROS may control different aspects of pollen differentiation.

Our results are consistent with other recent studies that indicated that ROS are a central signaling molecule at the junction

of different signaling pathways that mediate pollen tube growth and integrity. NADPH oxidase-derived ROS at the pollen tube tip were shown to dampen pollen tube growth rates, thereby allowing deposition of new cell wall material (6). This result suggests the intriguing possibility that increased ROS levels in the *are* mutant might greatly perturb coordination between pollen tube growth and cell wall deposition at the tip, thereby compromising cell wall integrity. NADPH oxidases are regulated by the Rho-related GTPase from plants (ROP) signaling pathway (46, 47). In pollen tubes, the ROP signaling pathway is activated by pollen-specific receptor(-like) kinases through Rho guanine nucleotide exchange factors (RopGEFs) (48–50). Interestingly, mutations in different components of the ROP signaling pathway display *are* mutant-like phenotypes, including reduced pollen germination and tube length, as well as isotropic growth (swelling) at the pollen tube tip (see, for example, refs. 49–53).

NADPH oxidases at the pollen tube tip were shown to act downstream of the receptor-like kinases (RLKs) ANXUR1 and ANXUR2, which are localized to the plasma membrane at the pollen tube tip (54) and regulate pollen tube integrity. Interestingly, overexpression of the ANXUR RLKs in pollen tubes, which likely increased ROS through NADPH oxidase activation, resulted in reduced pollen germination and swollen tube tips (54). The ANXUR overexpression thus phenocopied the *are* mutant with its increased ROS levels. ANXUR overexpression also led to overaccumulation of vesicles and cell wall precursors inside the pollen tube (54). Accumulation of vesicles has also been observed in pollen tube tips of a flavonol-deficient petunia mutant (55), suggesting that increased ROS lead to perturbed trafficking toward the plasma membrane and membrane fusion. Based on recent advances in identification of signaling pathways involved in pollen tube growth and integrity, combined with our findings on flavonols as regulators of ROS levels in pollen tubes, we propose that flavonols regulate pollen tube integrity by dampening signaling by NADPH oxidase-dependent ROS signaling pathways, and pollen tube growth by controlling ROS produced in an NADPH oxidase-independent manner.

Male reproductive plant tissues are more sensitive to high-temperature stress than vegetative tissue, both during male gametophyte development and pollen tube growth (33–37). We found that prolonged heat stress during tomato pollen development inhibits pollen viability, with the inhibitory effect on *are* pollen being dramatically enhanced, consistent with the reduction in an important antioxidant defense system. High-temperature stress in vegetative tissues increases transcript abundance and enzyme activity of genes involved in ROS metabolism (39, 41), resulting in elevated ROS (39, 41, 56, 57), which causes oxidative damage to cellular macromolecules (11). However, ROS levels in heat-stressed reproductive tissues have not been widely examined. Several studies have suggested that flavonols are part of the heat-stress response in vegetative and reproductive tissues. Indeed, transcript abundances and enzyme activities of flavonol biosynthetic genes (39), as well as flavonol pools (39, 42), increase during heat stress in tomato leaves and pollen grains. Therefore, we analyzed the effect of acute heat stress on tomato pollen tube growth and ROS levels. Transfer of in vitro-grown pollen tubes to 34 °C for 2.5 h increased signal from a ROS sensor and reduced elongation of wild-type and *are* pollen tube growth, with more profound effects shown for *are* in both assays. To test if heat-stress–induced inhibition of tube growth was a ROS-dependent process, we reduced ROS levels by antioxidant treatment, which reversed the effect of elevated temperature on pollen tube growth in *are*, restoring growth to wild-type levels. Together, these results implicate flavonols as important scavengers of heat-induced ROS needed to protect plants from this damage.

In conclusion, we provide important mechanistic insights into how flavonols modulate pollen development at normal and increased temperatures, as outlined in a model in Fig. 7*E*. Our study demonstrates that flavonols play critical roles in pollen development and fertility in tomato. It reveals that flavonols act as antioxidants to regulate ROS levels, thereby modulating pollen production, viability, germination, and tube growth. Finally, we show that flavonols protect pollen from prolonged and acute temperature stress and from elevations of ROS during acute heat stress. Flavonols are therefore critical metabolites involved in the adaptation to heat stress and their synthesis is an excellent target for rational metabolic engineering in pollen to maintain or improve crop yields in a changing climate.

Materials and Methods

Plant Materials and Growth. Wild-type (VF36) and *are* mutant seeds were obtained from the Tomato Genetic Resource Center (https://tgrc.ucdavis.edu/). Transgenic lines expressing the *F3H* gene in the *are* mutant under the control of the CaMV *35S* promoter were generated by Maloney et al. (25). Plants were grown from seed to flowering in the greenhouse. The greenhouse temperature was set to 26 °C during the day and to 22 °C at night. For pollen viability quantification illustrated in Fig. 7*A*, pollen was harvested from plants grown in spring or summer. During the spring, the average day and night greenhouse temperatures measured 7–15 d before anthesis were 22 °C and 21 °C, respectively, while the average day and night temperatures in the summer were 37 °C and 25 °C, respectively. Temperatures were determined using a temperature monitoring sensor (Minus 80 Monitoring).

Pollen Viability Assay. Anthers were detached from flowers at anthesis and placed in a 5- or 15-mL conical tube. Pollen was released from the anthers by vortexing. The released pollen was resuspended in pollen viability solution [PVS, 290 mM sucrose, 1.27 mM $Ca(NO_3)_2$, 0.16 mM boric acid, 1 mM KNO_3) containing 0.001% (wt/vol) fluorescein diacetate, and 10 μM propidium iodide (stock solutions: 1% (wt/vol) fluorescein diacetate in acetone; 2 mM PI in water]. Pollen was stained for 15 min at 28 °C and then centrifuged. The PVS containing FDA and PI was replaced with PVS alone, the stained pollen placed on a microscope slide, and then imaged by confocal microscopy on a Zeiss 880 LSCM microscope. FDA was excited with a 488-nm laser and its signal collected at 493–584 nm. PI was excited with a 561-nm laser and its signal collected at 584–718 nm. Maximum laser power was 0.025% and 0.02% for FDA and PI, respectively. Quantification of viable and dead pollen grains was performed using Fiji (58).

Quantification of Pollen Grains by Flow Cytometry. Anthers from three flowers were detached at anthesis and placed in a 5-mL conical tube. Pollen was released from the anthers by vortexing. Anthers were removed from the tube and the released pollen resuspended in 310-μL PVS containing 50,000 CountBright Absolute Counting Beads (ThermoFisher). Pollen grains were quantified by analyzing a known volume of pollen grain-containing solution by flow cytometry (BD Accuri C6 Analyzer) using forward and sideways scatter to quantify grains and differentiate pollen grains and beads. To account for differences in flow between flow-cytometry runs, pollen counts were normalized by the number of counting beads measured in each run.

Pollen Tube Germination, Growth, and Integrity Assays and Temperature-Stress Experiments. Pollen grains were harvested as described above and resuspended in pollen germination medium [PGM: 24% (wt/vol) PEG4000, 0.01 (wt/vol) boric acid, 2% (wt/vol) sucrose, 20 mM Hepes pH 6.0, 30 mM $Ca(NO_3)_2$, 0.02% (wt/vol) $MgSO_4$, 0.01% (wt/vol) KNO_3]. The pollen in PGM was transferred to a 24-well plate and incubated at 28 °C for 4 h. For heat-stress treatment, pollen in PGM was incubated at 28 °C for 1.5 h and then at 34 °C for 2.5 h.

Chemical inhibition of NADPH oxidase was achieved by adding DPI (0.05, 0.25 and 1.25 mM stock solutions in DMSO; 0.5-, 2.5-, and 12.5-μM final concentrations) to growing pollen tubes germinated for 1.5 h in unsupplemented PGM. The solvent control consisted of an equivalent volume of DMSO as used in the DPI treatments. Ascorbic acid treatments were performed using 25-, 50-, and 100-mM stock solutions in water that were diluted to 250-, 500-, and 1,000-μM final concentrations) which were added to growing pollen tubes germinated for 1.5 h in unsupplemented PGM. The solvent control consisted of an equivalent volume of water as used in the ascorbic acid treatments.

Pollen tubes were imaged by bright-field illumination using an inverted Olympus IX83 microscope equipped with a digital CMOS camera (ORCA-FLASH4.0; Hamamatsu). Images were taken with a 4× objective. Temperature during imaging was controlled using an AirTherm SMT system (World Precision Instrument) and a custom-built microscope enclosure.

Quantification of pollen tube length was performed using in Fiji (58). Pollen tube integrity, as judged by quantifying the percentage of intact pollen tubes, was assessed in images captured for analysis of pollen tube length.

DPBA Staining of Pollen Grains and Tubes. Pollen grains were harvested as described above and resuspended in PVS containing 2.5 mg/mL DPBA (Sigma-Aldrich) and 0.005% (vol/vol) Triton X-100. Pollen was stained for 20 min at 28 °C and then centrifuged. The PVS containing DPBA and Triton X-100 was replaced with PVS alone, the stained pollen affixed on a microscope slide, and then imaged by confocal microscopy on a Zeiss 880 LSCM microscope. Pollen tubes were grown in PGM for 2 h on a 35-mm glass-bottom dish coated with poly-D-lysine. After 2 h, PGM was replaced with PGM containing 2.5 mg/mL DPBA and 0.005% (vol/vol) Triton X-100 and pollen tubes incubated for another 20 min at 28 °C. Tubes were then imaged by confocal microscopy on a Zeiss 880 LSCM microscope.

DPBA in grains and tubes was excited with 0.025% maximum laser power at 458 nm and fluorescence collected between 472 and 615 nm. The gain settings were selected to maximize DPBA signal intensity in VF36 while preventing signal saturation. Grains and tubes were imaged with a pinhole of 1 Airy unit. Sequences of *z*-stack images were acquired for pollen tubes. All images for VF36 and the *are* mutant of each biological replicate were acquired using identical laser, pinhole, gain, and offset settings. Laser power and gain were adjusted between different biological replicates. Nonstained samples were used to verify the absence of autofluorescence with the fluorescence-capture settings used for DPBA imaging.

Quantification of DPBA fluorescence intensity was performed in Fiji (58). Images of maximum intensity projections produced from *z*-stacks were used for fluorescence quantifications in tubes. Regions of interest (ROI) for DPBA fluorescence quantification in grains were defined as the area within the perimeter of the ungerminated grain, while they were restricted to the tube only for DPBA fluorescence quantification in pollen tubes. Average fluorescence intensities within each ROI were used for statistical analyses.

CM-H_2DCFDA, PO1, and FDA Staining of Pollen Grains and Tubes. Pollen grains were harvested as described above and resuspended in PVS containing 5 μM CM-H_2DCFDA (stock solution: 500 μM CM-H_2DCFDA in DMSO; ThermoFisher). Pollen was stained for 20 min at 28 °C and then centrifuged. The PVS containing CM-H_2DCFDA was replaced with PVS alone, the stained pollen affixed on a microscope slide for imaging. Pollen tubes were grown in PGM for 2 h on a 35-mm glass-bottom dish coated with poly-D-lysine. After 2 h, PGM was replaced with PGM containing 5 μM CM-H_2DCFDA and pollen tubes incubated for another 20 min at 28 °C. Grains and tubes were then imaged by confocal microscopy on a Zeiss 880 LSCM microscope. Staining with PO1 (Tocris Bioscience) and FDA was performed as described for CM-H_2DCFDA. However, final concentrations for PO1 and FDA were 5 μM and 0.001% (wt/vol), respectively.

Laser settings for CM-H_2DCFDA and FDA were the following: CM-H_2DCFDA and FDA were excited with a 488-nm laser with 0.02% maximum laser power and fluorescence collected between 490 and 606 nm. For PO1, the excitation wavelength was 488 nm with 0.025% maximum laser power and the emission wavelengths were collected between 544 and 624 nm. Nonstained samples were used to verify absence of autofluorescence with the fluorescence-capture settings used for CM-H_2DCFDA, PO1, and FDA imaging. Quantification of CM-H_2DCFDA, PO1, and FDA fluorescence intensity in ungerminated pollen grains and pollen tubes was performed as described above for DPBA fluorescence intensity.

Statistical Analysis. All of the data were analyzed using the statistical software GraphPad Prism 7. A Student's *t* test was performed to detect statistical differences between VF36 and the *are* mutant. An ANOVA with a Šídák post hoc test was used to compare VF36, the *are* mutant, and the *are-F3H* complemented lines. A two-way ANOVA followed by a Fisher's post hoc test was used in all other analyses. Each figure legend describes the statistical tests employed to analyze the illustrated data.

ACKNOWLEDGMENTS. We thank Dr. Greg Maloney for his original observations that inspired this work; Dr. Mark Johnson (Brown University) and G.K.M. laboratory members for editorial comments; Dr. Glenn Marrs and Dr. Heather Brown-Harding (Wake Forest University) for their help with microscopy; Dr. Pierre-Alexandre Vidi (Wake Forest School of Medicine) for providing access to the Olympus IX83 microscope; and Dr. Martha Alexander-Miller and the Wake Forest School of Medicine Flow Cytometry Core facility for their assistance. This project was supported by the United States Department of Agriculture National Institute of Food and Agriculture program and the Agriculture and Food Research Initiative in a foundational Grant 2015-06811 (to G.K.M.); by the Swiss National Science Foundation in a postdoctoral fellowship P2SKP3_161684 (to J.K.M); and by the Wake Forest University Undergraduate Research and Creative Activities Center in an undergraduate research fellowship (to T.L.B.Y.).

1. Cheung AY, Boavida LC, Aggarwal M, Wu HM, Feijó JA (2010) The pollen tube journey in the pistil and imaging the in vivo process by two-photon microscopy. *J Exp Bot* 61: 1907–1915.
2. Xie HT, Wan ZY, Li S, Zhang Y (2014) Spatiotemporal production of reactive oxygen species by NADPH oxidase is critical for tapetal programmed cell death and pollen development in Arabidopsis. *Plant Cell* 26:2007–2023.
3. Smirnova AV, Matveyeva NP, Yermakov IP (2014) Reactive oxygen species are involved in regulation of pollen wall cytomechanics. *Plant Biol (Stuttg)* 16:252–257.
4. Speranza A, Crinelli R, Scoccianti V, Geitmann A (2012) Reactive oxygen species are involved in pollen tube initiation in kiwifruit. *Plant Biol (Stuttg)* 14:64–76.
5. Kaya H, et al. (2014) Ca2+-activated reactive oxygen species production by Arabidopsis RbohH and RbohJ is essential for proper pollen tube tip growth. *Plant Cell* 26: 1069–1080.
6. Lassig R, Gutermuth T, Bey TD, Konrad KR, Romeis T (2014) Pollen tube NAD(P)H oxidases act as a speed control to dampen growth rate oscillations during polarized cell growth. *Plant J* 78:94–106.
7. Potocký M, Jones MA, Bezvoda R, Smirnoff N, Zárský V (2007) Reactive oxygen species produced by NADPH oxidase are involved in pollen tube growth. *New Phytol* 174: 742–751.
8. Duan Q, et al. (2014) Reactive oxygen species mediate pollen tube rupture to release sperm for fertilization in *Arabidopsis*. *Nat Commun* 5:3129.
9. Guan Y, Guo J, Li H, Yang Z (2013) Signaling in pollen tube growth: Crosstalk, feedback, and missing links. *Mol Plant* 6:1053–1064.
10. Møller IM, Jensen PE, Hansson A (2007) Oxidative modifications to cellular components in plants. *Annu Rev Plant Biol* 58:459–481.
11. Mittler R (2002) Oxidative stress, antioxidants and stress tolerance. *Trends Plant Sci* 7: 405–410.
12. Winkel-Shirley B (2001) Flavonoid biosynthesis. A colorful model for genetics, biochemistry, cell biology, and biotechnology. *Plant Physiol* 126:485–493.
13. Hernández I, Alegre L, Van Breusegem F, Munné-Bosch S (2009) How relevant are flavonoids as antioxidants in plants? *Trends Plant Sci* 14:125–132.
14. Pourcel L, Routaboul JM, Cheynier V, Lepiniec L, Debeaujon I (2007) Flavonoid oxidation in plants: From biochemical properties to physiological functions. *Trends Plant Sci* 12:29–36.
15. Appelhagen I, et al. (2014) Update on transparent testa mutants from *Arabidopsis thaliana*: Characterisation of new alleles from an isogenic collection. *Planta* 240: 955–970.
16. Gayomba SR, Watkins JM, Muday GK (2016) Flavonols regulate plant growth and development through regulation of auxin transport and cellular redox status. *Recent Advances in Polyphenol Research*, eds Yoshida K, Cheynier V, Quideau S (John Wiley & Sons, Chichester, UK).
17. Buer CS, Djordjevic MA (2009) Architectural phenotypes in the *transparent testa mutants* of *Arabidopsis thaliana*. *J Exp Bot* 60:751–763.
18. Buer CS, Kordbacheh F, Truong TT, Hocart CH, Djordjevic MA (2013) Alteration of flavonoid accumulation patterns in *transparent testa* mutants disturbs auxin transport, gravity responses, and imparts long-term effects on root and shoot architecture. *Planta* 238:171–189.
19. Buer CS, Muday GK (2004) The *transparent testa4* mutation prevents flavonoid synthesis and alters auxin transport and the response of *Arabidopsis* roots to gravity and light. *Plant Cell* 16:1191–1205.
20. Lewis DR, et al. (2011) Auxin and ethylene induce flavonol accumulation through distinct transcriptional networks. *Plant Physiol* 156:144–164.
21. Ringli C, et al. (2008) The modified flavonol glycosylation profile in the *Arabidopsis rol1* mutants results in alterations in plant growth and cell shape formation. *Plant Cell* 20:1470–1481.
22. Kuhn BM, et al. (2016) 7-Rhamnosylated flavonols modulate homeostasis of the plant hormone auxin and affect plant development. *J Biol Chem* 291:5385–5395.
23. Watkins JM, Hechler PJ, Muday GK (2014) Ethylene-induced flavonol accumulation in guard cells suppresses reactive oxygen species and moderates stomatal aperture. *Plant Physiol* 164:1707–1717.
24. Watkins JM, Chapman JM, Muday GK (2017) Abscisic acid-induced reactive oxygen species are modulated by flavonols to control stomata aperture. *Plant Physiol* 175: 1807–1825.
25. Maloney GS, DiNapoli KT, Muday GK (2014) The *anthocyanin reduced* tomato mutant demonstrates the role of flavonols in tomato lateral root and root hair development. *Plant Physiol* 166:614–631.
26. Mo Y, Nagel C, Taylor LP (1992) Biochemical complementation of chalcone synthase mutants defines a role for flavonols in functional pollen. *Proc Natl Acad Sci USA* 89: 7213–7217.

27. Pollak PE, Vogt T, Mo Y, Taylor LP (1993) Chalcone synthase and flavonol accumulation in stigmas and anthers of *Petunia hybrida*. *Plant Physiol* 102:925–932.
28. Schijlen EG, et al. (2007) RNA interference silencing of chalcone synthase, the first step in the flavonoid biosynthesis pathway, leads to parthenocarpic tomato fruits. *Plant Physiol* 144:1520–1530.
29. Ylstra B, et al. (1992) Flavonols stimulate development, germination, and tube growth of tobacco pollen. *Plant Physiol* 100:902–907.
30. Ylstra B, Muskens M, Van Tunen AJ (1996) Flavonols are not essential for fertilization in *Arabidopsis thaliana*. *Plant Mol Biol* 32:1155–1158.
31. Burbulis IE, Iacobucci M, Shirley BW (1996) A null mutation in the first enzyme of flavonoid biosynthesis does not affect male fertility in *Arabidopsis*. *Plant Cell* 8: 1013–1025.
32. Dupuis I, Dumas C (1990) Influence of temperature stress on in vitro fertilization and heat shock protein synthesis in maize (*Zea mays* L.) reproductive tissues. *Plant Physiol* 94:665–670.
33. Snider JL, Oosterhuis DM (2011) How does timing, duration and severity of heat stress influence pollen-pistil interactions in angiosperms? *Plant Signal Behav* 6:930–933.
34. Snider JL, Oosterhuis DM, Loka DA, Kawakami EM (2011) High temperature limits in vivo pollen tube growth rates by altering diurnal carbohydrate balance in field-grown *Gossypium hirsutum* pistils. *J Plant Physiol* 168:1168–1175.
35. Sato S, et al. (2006) Moderate increase of mean daily temperature adversely affects fruit set of *Lycopersicon esculentum* by disrupting specific physiological processes in male reproductive development. *Ann Bot* 97:731–738.
36. Sato S, Peet MM, Thomas JF (2002) Determining critical pre- and post-anthesis periods and physiological processes in *Lycopersicon esculentum* Mill. exposed to moderately elevated temperatures. *J Exp Bot* 53:1187–1195.
37. Pressman E, Peet MM, Pharr DM (2002) The effect of heat stress on tomato pollen characteristics is associated with changes in carbohydrate concentration in the developing anthers. *Ann Bot* 90:631–636.
38. Willems P, et al. (2016) The ROS wheel: Refining ROS transcriptional footprints. *Plant Physiol* 171:1720–1733.
39. Martinez V, et al. (2016) Accumulation of flavonols over hydroxycinnamic acids favors oxidative damage protection under abiotic stress. *Front Plant Sci* 7:838.
40. Rainwater DT, et al. (1996) The relationship between yield and the antioxidant defense system in tomatoes grown under heat stress. *Free Radic Res* 25:421–435.
41. Suzuki N, Mittler R (2006) Reactive oxygen species and temperature stresses: A delicate balance between signaling and destruction. *Physiol Plant* 126:45–51.
42. Paupière MJ, et al. (2017) Untargeted metabolomic analysis of tomato pollen development and heat stress response. *Plant Reprod* 30:81–94.
43. De Jong WS, Eannetta NT, De Jong DM, Bodis M (2004) Candidate gene analysis of anthocyanin pigmentation loci in the Solanaceae. *Theor Appl Genet* 108:423–432.
44. Yoder JI, Belzile F, Tong Y, Goldsbrough A (1994) Visual markers for tomato derived from the anthocyanin biosynthetic pathway. *Euphytica* 79:163–167.
45. Taylor LP, Jorgensen R (1992) Conditional male fertility in chalcone synthase-deficient petunia. *J Hered* 83:11–17.
46. Wong HL, et al. (2007) Regulation of rice NADPH oxidase by binding of Rac GTPase to its N-terminal extension. *Plant Cell* 19:4022–4034.
47. Duan Q, Kita D, Li C, Cheung AY, Wu HM (2010) FERONIA receptor-like kinase regulates RHO GTPase signaling of root hair development. *Proc Natl Acad Sci USA* 107: 17821–17826.
48. Kaothien P, et al. (2005) Kinase partner protein interacts with the LePRK1 and LePRK2 receptor kinases and plays a role in polarized pollen tube growth. *Plant J* 42: 492–503.
49. Zhang Y, McCormick S (2007) A distinct mechanism regulating a pollen-specific guanine nucleotide exchange factor for the small GTPase Rop in *Arabidopsis thaliana*. *Proc Natl Acad Sci USA* 104:18830–18835.
50. Chang F, Gu Y, Ma H, Yang Z (2013) AtPRK2 promotes ROP1 activation via RopGEFs in the control of polarized pollen tube growth. *Mol Plant* 6:1187–1201.
51. Zhu L, et al. (2018) The *Arabidopsis* CrRLK1L protein kinases BUPS1 and BUPS2 are required for normal growth of pollen tubes in the pistil. *Plant J* 95:474–486.
52. Lin Y, Yang Z (1997) Inhibition of pollen tube elongation by microinjected anti-Rop1Ps antibodies suggests a crucial role for Rho-Type GTPases in the control of tip growth. *Plant Cell* 9:1647–1659.
53. Luo N, et al. (2017) Exocytosis-coordinated mechanisms for tip growth underlie pollen tube growth guidance. *Nat Commun* 8:1687.
54. Boisson-Dernier A, et al. (2013) ANXUR receptor-like kinases coordinate cell wall integrity with growth at the pollen tube tip via NADPH oxidases. *PLoS Biol* 11: e1001719.
55. Derksen J, van Wezel R, Knuiman B, Ylstra B, van Tunen AJ (1999) Pollen tubes of flavonol-deficient petunia show striking alterations in wall structure leading to tube disruption. *Planta* 207:575–581.
56. Volkov RA, Panchuk II, Mullineaux PM, Schöffl F (2006) Heat stress-induced $H_{(2)}O_{(2)}$ is required for effective expression of heat shock genes in *Arabidopsis*. *Plant Mol Biol* 61:733–746.
57. Weston DJ, et al. (2011) Comparative physiology and transcriptional networks underlying the heat shock response in *Populus trichocarpa*, *Arabidopsis thaliana* and *Glycine max*. *Plant Cell Environ* 34:1488–1506.
58. Schindelin J, et al. (2012) Fiji: An open-source platform for biological-image analysis. *Nat Methods* 9:676–682.